SUPPLEMENTAL MATERIAL

METHODS

Tractography analysis

Diffusion images were preprocessed according to previous methods (Berhens *et al.*, 2007; Keezele *et al.*, 2010; Tournier *et al.*, 2007) and processed for probabilistic diffusion tractography with MRtrix (http://www.brain.org.au/software/mrtrix/). Raw diffusion-weighted data were corrected for motion and geometric distortions secondary to eddy currents using a registration technique based upon the geometric model of distortions (Mangin *et al.*, 2002). The fibre orientation distribution function (ODF) was estimated using the constrained spherical deconvolution (CSD) method (Tournier et al., 2004, 2007) in MRtrix. The sufficient angular resolution allowed high-order fibre orientation estimation algorithms (Tuch *et al.*, 2002; Jansons and Alexander, 2003; Tournier *et al.*, 2004). The ODF information obtained from CSD was used with a suitable fibre-tracking algorithm to infer connectivity of crossing fibres. We used a probabilistic streamlines algorithm with the entire ODF as a probability density function (ODF threshold = 0.1; step size = 0.2 mm as 1/10 of the voxel size; radius of curvature = 1mm; up-sampling of DWI data to 1mm). In the native individual space, we performed a seed-to-target analysis from regions of interest defined along the CTC loop (see Regions of interest section for information on region of interest definition). An additional analysis was performed to verify the integrity of corticospinal pathways supporting the transmission of the motor output to hand muscles using the same tractography model. We used a probabilistic tractography algorithm: the number of fibres connecting a seed voxel to a target voxel was calculated by sampling one million draws for each fiber connection the seed to the target.

The CDTC, intracortical and corticospinal tracts were reconstructed for each subject. The cerebellar component of the CDTC tract included fibres connecting the cerebellar lobules involved in motor functions (lobules VI and VIII) and the dentate, excluding fibres passing through the opposite cerebellar hemisphere. The dentate-thalamic component of the CDTC tract included the dentate and the VIM of the opposite hemisphere, including the pedunculus ipsilateral to the dentate and excluding the cerebellar hemisphere contralateral to the dentate. The brain component of the CDTC tract included the ventro-lateral nucleus of the thalamus and one of the cortical targets (hand area of M1, or the anterior part of SMA proper), excluding the internal capsule, the striatum and the corpus callosum. The intracortical tract included fibres included fibres connecting the secondary motor cortex and the primary motor cortex within one hemisphere, excluding the corpus callosum, the striatum, the thalamus and the internal capsule. The cortico-spinal tracts included the internal capsule and one of the cortical targets, excluding the thalamus, the striatum and the corpus callosum.

After the tracts were reconstructed, the statistical analyses were performed on three different measures. For the uncrossed tracks, which had short trajectories (cortico-cortical, and cerebello-dentate tracts), a single mean FA value of all the voxel included in the tract was obtained after the normalization on the tracts in the MNI space. For the uncrossed tracks that had long trajectories (thalamo-cortical, and cortico-spinal tracts), the mean FA value was weighted by the probability of connection in each voxel of an area of interest specific to each tract. For the thalamo-cortical tracts, the area of interest contained the VL nucleus of the thalamus. For the corticospinal tracts, the area of interest contained the territory of the internal capsule traversed by fibers connecting the cortical representation of the hand muscle in the primary and secondary motor areas which did not overlap (see Figure 2). Comparisons between groups (ET, HV) were performed using a two sample t-test performed on the mean FA values or mean FA value weighted by the probability of connection depending on the

tract. Group differences were considered significant at $p<0.05$ corrected for the number of comparisons. For the crossed tracts that had long trajectories (dentate-thalamic tracts), the mean FA value for all the voxel included in the tract is not representative. Indeed, lower FA values are usually observed at the location of crossing fibres, which increases the variability of FA values in the whole tract. Thus, several mean FA values along the track were obtained based on B-spline resampling of the fibres and averaging the FA values for each individual fibre at the same location (elastic model with 30 points in space at analogous anatomical locations in each individual) (Colby *et al.* 2012). The statistical analysis followed the method described by Colby and collaborators (2012). Firstly, cross-sectional mean FA and variance estimates obtained on the 30 points along the mean fibre were fit in a linear mixed-effects model using R (http://www.r-project.org) to check for global difference on the whole tract. Secondly, mean FA values were also compared at each point of the mean fibre along the Z axis to check for local difference at specific points of the tract, using a statistical threshold at $p<0.05$ corrected for the number of comparisons.

Resting state fMRI

Low frequency fluctuations (LFF) are mainly within the 0.01–0.08 Hz range (Biswal et al., 1995; Cordes et al., 2001). Thus, we used the sinusoid functions in this range, with only 0.01, 0.02, 0.04, and 0.08 Hz, to cover the entire spectrum of the signal. Eight box-car functions were included as regressors in the GLM model to capture the LFF signals. The box-car functions used modeled cycle of 100, 50, 25, and 12.5 s (representing 0.01, 0.02, 0.04, and 0.08 Hz, respectively and built using matlab). These box-car functions corresponded to binarized versions of the sinusoidal Fourier components used. There were two box-car functions for each frequency with 90 degree phase delay between the two (see Di and Biswal, 2014 for more details). The box-car functions were not convolved with the hemodynamic

response functions (HRF). Six head motion parameters were also added into the model to remove potential confounding variances caused by head motion. The GLM model also includes an implicit high pass filter of 1/100 Hz, to remove ultraslow fluctuations that were due to scanner drift. After estimation of the GLM model, a diagonal F-contrast of all the eight regressors was used to obtain the regions whose variance of LFF could be significantly accounted for by the inclusion of the binarized Fourier series regressors.

The DCM analyses were conducted using the DCM10 routine implemented in the SPM8. For each subject, the first eigenvectors were extracted from the regions of interest after removing the effect of head motion, low frequency drift, white matter volume and CSF signals. The main purpose of the current DCM analysis was to investigate the endogenous effective connectivity. The modeled LFFs were set as driving input to all the regions of interest, and different models were defined by varying only the endogenous connectivity parameters A.

Correlation between GM changes and ALFF

We performed a pair-wise correlation analysis to assess the relationship between GM changes and ALFF changes in the cortical motor area (Pearson correlation coefficient significant at $p<0.05$, after verification of the normal distribution of the data).

RESULTS

Tractography analysis

There was no group effect for the mean FA value within bilateral dentate nucleus ($p=0.58$) or for the volumes of the cerebellar peduncles ($p=0.73$), which were used as ROIs to reconstruct the fibre tracts between each dentate and contralateral VIM thalamic nuclei.

For the crossed tracts, the dentate-thalamic tract showed no difference over all the data points ($F=0.85$, $p=0.68$). There was a tendency towards lower mean FA in patients compared to HV at the level of the left cerebellar pedunculi (Supplemental Figure 2), but this difference did not reach significance ($T=3.97$, $p=0.09$ uncorrected for multiple comparisons).

DCM Analysis

The Bayesian model comparison showed that the simple models (unilateral connections) were the best fit given the data (posterior exceedance probabilities = 0.98) compared to the complex models (bi-directional connections) for both groups separately (see Supplemental Figure 1B).

While extracting the intrinsic parameters for each connection of the cerebello-thalamic and the thalamo-cortical models, we ensured that the intrinsic parameters were significantly different from zero. The results of the one sample t-tests in the control group showed i) only the connection from SMA to M1 was significantly different from zero for the thalamo-cortical models (left hemisphere: $p=0.0001$; right hemisphere: $p=0.0002$; Figure 3B); ii) only the connection from cerebellar lobule VIII to the dentate, and from the dentate to the opposite VIM were significantly different from zero for the cerebello-dentato-thalamic models (left cerebellum → right VIM: $0.001<p<0.04$; right cerebellum → left VIM: $0.00006<p<0.01$; Figure 3B). In the patient group, only the connection from SMA to M1 of the left hemisphere ($p=0.04$) and the connections from the right cerebellar lobule VIII to the right dentate ($p=0.03$), and from the right dentate to the left VIM ($p=0.002$) were significantly different from zero.

Correlation between GM changes and ALFF in SMA

A significant correlation was found between the loss of GM volume in the left cerebellum and the right SMA proper A significant correlation was found between GM volume and the ALFF in the SMA proper: the greater the GM volume, the lower the ALFF (Supplemental Figure 3).

REFERENCES

Behrens TEJ, Berg, HJ, Jbabdi S, Rushworth MFS, and Woolrich MW. Probabilistic diffusion tractography with multiple fibre orientations: What can we gain? Neuroimage 2007; 34: 144–155.

Biswal BB, Mennes M, Zuo XN, Gohel S, Kelly C, Smith SM et al. Toward discovery science of human brain function. Proc Natl Acad Sci U S A. 2010;107(10):4734–4739.

Cordes D., Haughton V.M., Arfanakis K., Carew J.D., Turski P.A., Moritz C.H., Quigley M.A., Meyerand ME. Frequencies contributing to functional connectivity in the cerebral cortex in "resting-state" data. AJNR Am J Neuroradiol. 2001; 22:1326–33.

Di X, Biswal BB. Identifying the default mode network structure using dynamic causal modeling on resting-state functional magnetic resonance imaging. NeuroImage 2014; 86: 53–59.

Kezele I, Descoteaux M, Poupon C, Poupon F, Mangin JF. Spherical wavelet transform for ODF sharpening. Med Image Anal. 2010;14:332-342.Mangin JF, Poupon C, Clark C, Le Bihan D, Bloch I. Distortion correction and robust tensor estimation for MR diffusion imaging. Med Image Anal. 2002 Sep;6(3):191-8.

Nachev P, Kennard C, Husain M. Functional role of the supplementary and pre-supplementary motor areas. Nat. Rev. Neurosci. 2008; 9: 856–869.

Stephan KE, Penny WD, Daunizeau J, Moran RJ, and Friston KJ. Bayesian model selection for group studies. Neuroimage 2009; 46, 1004–1017.

Stephan KE, Penny WD, Moran RJ, den Ouden HEM, Daunizeau J, and Friston KJ. Ten simple rules for dynamic causal modeling. Neuroimage 2010; 49, 3099–3109.

Tournier J-D, Calamante F, and Connelly A. Robust determination of the fibre orientation distribution in diffusion MRI: non-negativity constrained super-resolved spherical deconvolution. Neuroimage 2007; 35, 1459–1472.

Tournier J-D, Calamante F, Gadian DG, and Connelly A. Direct estimation of the fiber orientation density function from diffusion-weighted MRI data using spherical deconvolution. Neuroimage 2004; 23, 1176–1185.

Tuch DS, Reese TG, Wiegell MR, Makris N, Belliveau JW, Wedeen VJ. High angular resolution diffusion imaging reveals intravoxel white matter fiber heterogeneity. Magn Reson Med. 2002;48: 577-582.

LEGENDS OF THE SUPPLEMENTARY FIGURES

Supplemental Figure 1. DCM models and Bayesian model selection (BMS). (A) Alternative models testing the cerebellar influence on the thalamus, the thalamic influence on the cortical motor areas, and the contribution of SMA to modulate M1 activity. M1 = primary motor cortex, SMA = supplementary motor area, VLA = ventro-lateral anterior nucleus of the thalamus, VIM = ventral-intermediate nucleus of the thalamus, VI = cerebellar lobule VI, VIII = cerebellar lobule VIII, L = left, R = right. Simple models involved unidirectional connections, whereas complex models involved bidirectional connections. (B) Results of the Bayesian model selection in both healthy volunteers (HV) and ET patients showing the model that most likely fits the data. In the Bayesian approach, the expected probability represents the best balance between model complexity and how the model fits the data. Family involved the two symmetrical models (for instance for the simple thalamo-cortical models, the left and the right hemisphere models were included in one family).

Supplemental Figure 2. Tractography results in the CDTC track. A. ROIs (color blobs superimposed on an individual anatomical image, left side of each panel) of the cerebellar lobule VIII (VIIIa in blue, VIIIb in red), the lobule VI (cyan) and the dentate (yellow) included in the cerebello-dentate tracks (individual tract superimposed on an individual FA map, right side of each panel). Diagrams represent the mean FA and standard error in the patient group (light color) and the healthy volunteer group (dark color). B. ROIs (color blobs superimposed on an individual anatomical image, upper part of the black panel) of the dentate (yellow) and the VIM (green) included in the dentate-thalamic tracks (mean “spaghetti” fiber, lower part of the black panel). Plots represent the mean FA along cross-sectional Z axis in the dentate-thalamic track (red = patients; blue = healthy volunteers) and standard deviation (darker grey area) within each group.

Supplemental Figure 3. Results of pair-wise correlation. Correlation between GM volume in the cerebellum (extracted from the VBM analysis, Figure 1A) and the GM volume in the SMA proper (extracted from the VBM analysis, Figure 1A). Correlation between GM volume (extracted from the VBM analysis, Figure 1A) and the ALFF (extracted from the resting state analysis (Figure 2A) in the bilateral SMA proper.

Supplemental Figure 1

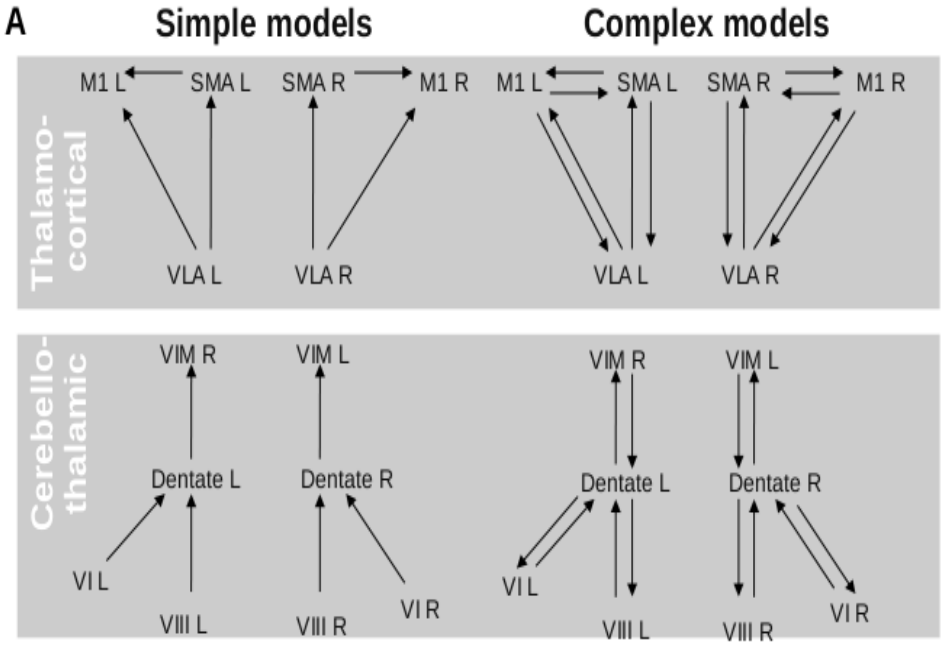

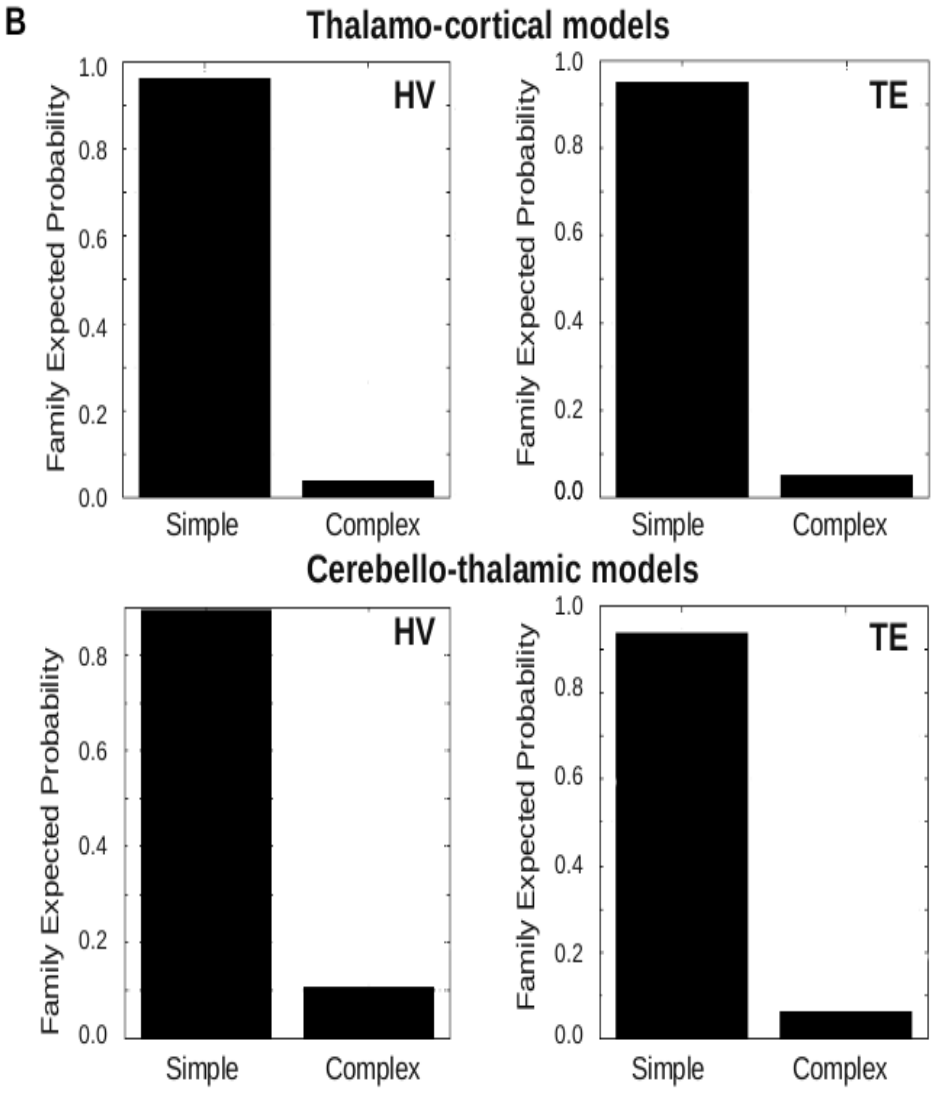

Supplemental Figure 2

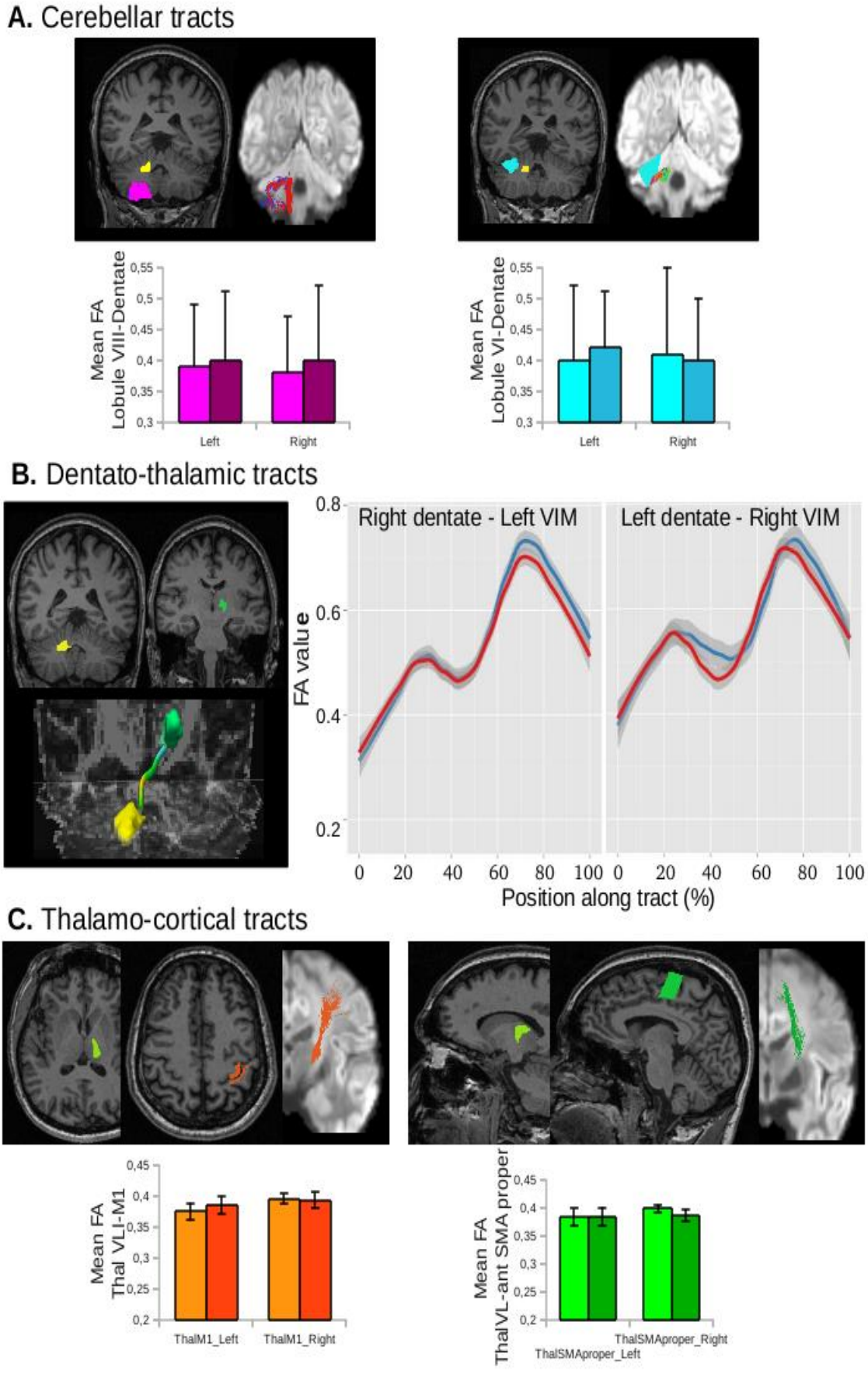

Supplemental Figure 3